
The Effects of Local Spring Perch Flexibility on Suspension Geometry of a Winston Cup Race Car

Lonny L. Thompson, Gregory P. Herrick and E. Harry Law
Clemson Univ.

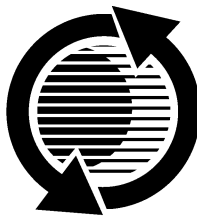
Reprinted From: **1998 Motorsports Engineering Conference Proceedings**
Volume 1: Vehicle Design and Safety
(P-340/1)

The appearance of this ISSN code at the bottom of this page indicates SAE's consent that copies of the paper may be made for personal or internal use of specific clients. This consent is given on the condition, however, that the copier pay a \$7.00 per article copy fee through the Copyright Clearance Center, Inc. Operations Center, 222 Rosewood Drive, Danvers, MA 01923 for copying beyond that permitted by Sections 107 or 108 of the U.S. Copyright Law. This consent does not extend to other kinds of copying such as copying for general distribution, for advertising or promotional purposes, for creating new collective works, or for resale.

SAE routinely stocks printed papers for a period of three years following date of publication. Direct your orders to SAE Customer Sales and Satisfaction Department.

Quantity reprint rates can be obtained from the Customer Sales and Satisfaction Department.

To request permission to reprint a technical paper or permission to use copyrighted SAE publications in other works, contact the SAE Publications Group.



GLOBAL MOBILITY DATABASE

All SAE papers, standards, and selected books are abstracted and indexed in the Global Mobility Database

No part of this publication may be reproduced in any form, in an electronic retrieval system or otherwise, without the prior written permission of the publisher.

ISSN 0148-7191

Copyright 1998 Society of Automotive Engineers, Inc.

Positions and opinions advanced in this paper are those of the author(s) and not necessarily those of SAE. The author is solely responsible for the content of the paper. A process is available by which discussions will be printed with the paper if it is published in SAE Transactions. For permission to publish this paper in full or in part, contact the SAE Publications Group.

Persons wishing to submit papers to be considered for presentation or publication through SAE should send the manuscript or a 300 word abstract of a proposed manuscript to: Secretary, Engineering Meetings Board, SAE.

Printed in USA

The Effects of Local Spring Perch Flexibility on Suspension Geometry of a Winston Cup Race Car

Lonny L. Thompson, Gregory P. Herrick and E. Harry Law

Clemson Univ.

Copyright © 1998 Society of Automotive Engineers, Inc.

ABSTRACT

In order to achieve predictable handling of a race car, local mounts connecting suspension components to the chassis should be sufficiently rigid to minimize unwanted local deflection which may adversely affect suspension geometry. In this work, the effects of local chassis flexibility of the spring perch on roll stiffness, tire camber change, and steer angle change are determined from a finite element model (FEM) of a Winston Cup race car. Details such as side gussets, supporting brackets, and local curvature of the frame rail spring pocket are included in a shell model of the spring perch. The local shell model of the spring perch is integrated with the global finite element stiffness model of the chassis and suspension consisting of an assembly of beam and shell elements.

A parametric study on the effects of thickness changes for seven different areas of the spring perch has been performed. Tire camber change, steer angle change, and chassis roll stiffness are plotted as a function of thickness variation for each of the seven perch areas. Results indicate that the surface with the most adverse affects on torsional stiffness, roll stiffness, and camber changes, resulting from reduced thickness, is the principal spring support plate. Stiffness increases may be achieved by increasing the thickness of the spring plate, spring pocket, and frame rail box beam, but the greatest benefits result from otherwise fortifying the spring pocket and box beam. The frame rail box beam and spring pocket exert tremendous influence on steer angle behavior, and can increase roll stiffness and minimize camber change if properly reinforced.

INTRODUCTION

Chassis stiffness is critical to the handling performance of NASCAR Winston Cup Race Cars. One parameter frequently used to quantify chassis stiffness is torsional stiffness: In this work, torsional stiffness relates the differential load inputs applied at the suspension attachment points to the overall deflection of these points. The overall deflection of these points is a summation of the

global behavior of the chassis and the local behavior of the suspension attachment points. A stiffer chassis deflects less at these load-bearing suspension attachment points, and in turn improves vehicle handling by allowing the suspension components to control a larger percentage of a vehicle's kinematics. Race teams have found that if they can reduce chassis deformation at the suspension attachment points, they can better control the handling of the car. This study will address the importance of local spring perch rigidity with regard to chassis torsional stiffness, front suspension roll stiffness, and camber and steer angles, due to differential load inputs.

In order to analyze the effects of local spring perch flexibility on chassis and suspension behavior, a structural finite element model has been constructed. The finite element models were constructed using I-DEAS software from SDRC [1]. Structural finite element models of Laughlin, Hopkins, and other modified Winston Cup chassis have previously been developed in [2,3]. These models employ beam elements for the tubular and box beam frame members and thin shell elements for the floor pan and firewall sheet metal. These models have been used to evaluate torsional stiffness of several competing chassis designs [4], and have aided in the design of a twist fixture used to measure torsional stiffness [5]. For this project, the Hopkins chassis model developed in [2] has been modified to contain a detailed thin shell model of the front suspension spring perches; this facilitates the analysis of local spring perch flexibility, impossible with previous models. This model will enable us to quantify the effects of local spring perch flexibility on chassis torsional stiffness and front suspension geometry. Parametric studies are performed to investigate the influence of front suspension spring perch surface thickness on the torsional stiffness of the chassis, as well as the effective roll stiffness of the flexible chassis in combination with the suspension components. The finite element model (FEM) will be used to determine the:

- local deflections present in the spring perch,
- torsional stiffness of the unsuspended chassis,
- roll stiffness of the chassis with attached front suspension,

- wheel camber and steer angle changes in the front suspension.

Results from the finite element analysis will help determine which surfaces of the spring perch must be robust, regardless of desires to reduce weight.

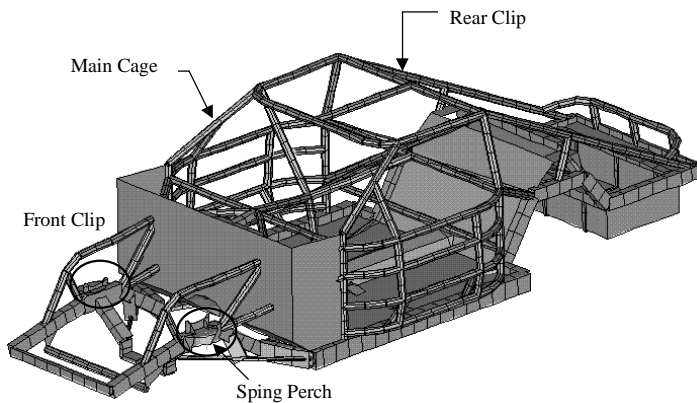


Figure 1. Isometric view of a Hopkins Winston Cup chassis highlighting the front spring perches.

FRONT SUSPENSION SPRING PERCHES

The focus of this study is the flexibility of the front spring perches located on the frame rails of the front clip, see Figures 1 and 2. Compression springs are mounted between the lower A-arms and the spring perches integrated with the frame rails of the chassis. On the top surfaces of the spring perch assemblies are the upper A-arm attachment plates and their supporting brackets. This upper A-arm attachment plate has a constant thickness; however, at the ears, the upper A-arms attach through a series of shims in order to adjust the A-arm position. The shims also serve to reinforce this load-bearing area. The upper spring perch allows for vertical adjustment of the springs using a threaded rod. By adjusting the upper spring perches, the amount of the vehicle's total weight supported by each tire can be controlled [6].

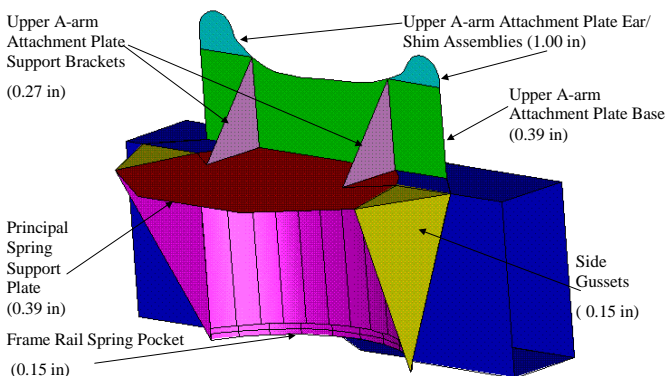


Figure 2. Description of areas of study on the front suspension spring perch (Numbers in parenthesis denote nominal thickness of the surface).

The spring perches consist of seven principal steel plate members; see Figure 2. The thickness of the various surfaces of the spring perches is given in Table I. The geometry and thickness of the spring perches were measured from a typical Winston Cup chassis [7]. To aid in visualization of the spring perch, a rapid prototype model was built using a stereolithography process in the Clemson Rapid Prototyping Lab, see Figure 3.

Table I. Nominal thickness of front suspension spring perch surfaces.

Spring Perch Surface	Nominal Thickness, in
Frame Rail Box Beam Wall	0.12
Principal Spring Support Plate	0.39
Side Gussets	0.15
Frame Rail Spring Pocket	0.15
Upper A-arm Attachment Plate Base	0.39
Upper A-arm Attachment Plate Support Bracket	0.27
Upper A-arm Attachment Plate Ear/ Shim Assembly	1.00

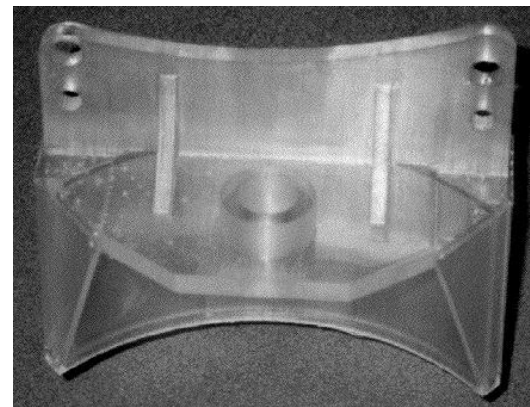


Figure 3. Stereolithography rapid prototype model of left spring perch.

In general, for Winston Cup chassis the driver side spring perch is considerably more robust than the passenger side. Projecting outward from the top surface of the frame rail is the principal spring support plate. Supporting this plate from the sides and from beneath are the side gussets. These side gussets also flank the concave frame rail spring pocket surface; this surface is made concave to accommodate the front suspension coil springs. The principal spring support plate projects outward less on the right side than the left side, and the upper A-arm attachment plate is shorter on the right side than the left side. Excessive deflection of the spring support plates and the upper A-arm attachment plates can adversely affect chassis torsional stiffness, roll stiffness, and tire camber and steer angle response.

FINITE ELEMENT MODEL OF CHASSIS AND SPRING PERCHES – Because the front suspension spring perch (with integrated frame rail) consists of thin plates and box beam surfaces, the finite element model employs thin shell elements, see Figures 4 and 5. A thin shell model provides for accurate prediction of the local deflections of the front suspension spring perch surfaces. To quantify the effects of local spring perch flexibility on roll stiffness and front suspension geometry, the thickness of each surface present in the front suspension spring perch is varied in a parametric study.

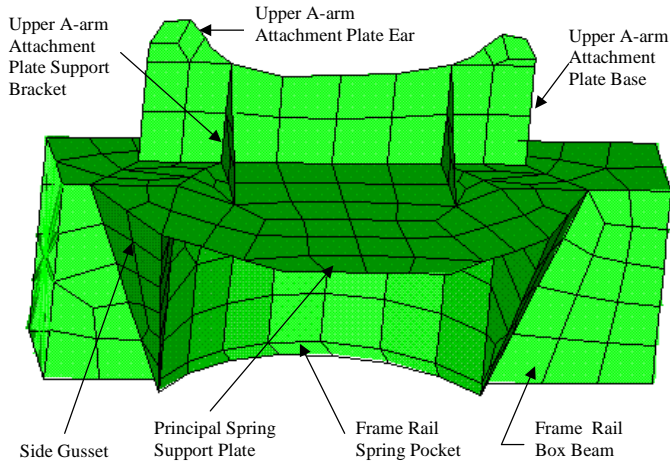


Figure 4. Finite Element Model of the left front suspension spring perch.

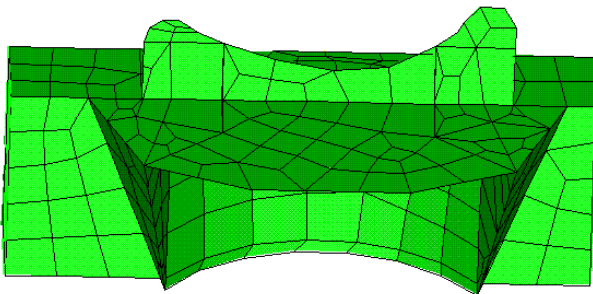


Figure 5. Finite element model of the right front suspension spring perch.

The geometry of the chassis model is based on measured data taken from a Hopkins chassis supplied by one of the race teams [2]. The chassis was measured by projecting the centers of the welded joints onto a surface plate to determine the x-y components of key-point positions. The heights of the key-points above the surface plate were measured to determine the z-coordinates. The chassis model was constructed of steel with Young's Modulus $E = 30 \times 10^6$ psi, and Poisson's Ratio $\nu = 0.3$. The chassis model is constructed using beam elements for the tubular members of the roll cage and front and rear clips. Thin shell elements are used to model the floor pan and firewall. Two alternative methods for integrating the detailed shell model of the front suspension spring perches with the chassis beam model are considered.

INTEGRATION OF LOCAL SPRING PERCH WITH GLOBAL CHASSIS MODEL – One approach to integrating the detailed shell model of the spring perch with the global chassis model is to mesh the entire box-beam frame assembly with similar shell elements as shown in Figure 6.

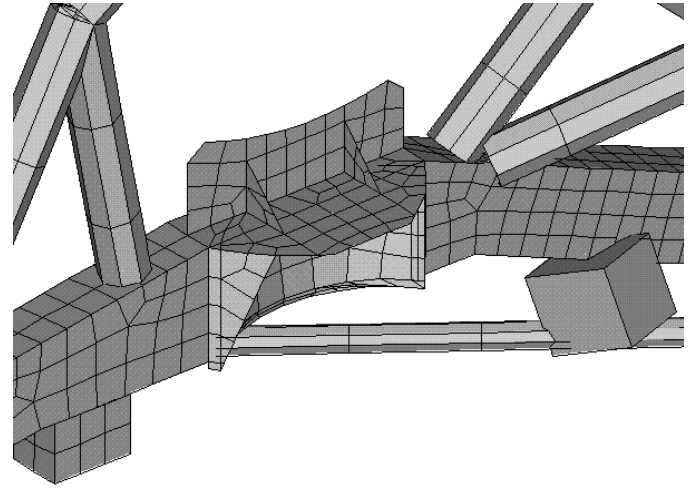


Figure 6. Full Shell Model for Frame Rails

In order to generate thin shell elements on each surface of the chassis box beams, a full solid/surface model of the frame rails, spring perch, floor pan, and firewall is required, as shown in Figure 7. Using this geometry, a thin shell finite elements can be placed on these surfaces using an automatic mesh generator available in state-of-the-art software, e.g. I-DEAS, see Figure 8. This modeling approach allows for accurate representation of frame rail geometry and ensures continuity of degrees-of-freedom (DOF) between the local spring perch and the global chassis model. However, it introduces difficulties in coupling beam elements representing the circular tube members of the roll-cage with the surfaces of the shell mesh of the box-beam frame rails. In this modeling approach, single node connections between beam elements and shell elements result in excessive deflection. In addition, an accurate mesh of shell elements representing all of the frame rails, floor pan and firewall required 13,036 nodes and 78,216 degrees of freedom, resulting in large computation times and storage requirements.

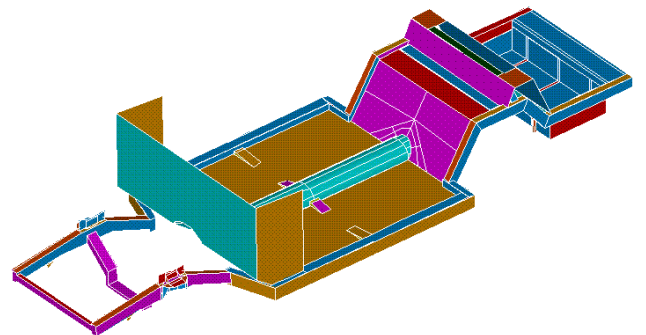


Figure 7. Solid/surface model of Hopkins chassis frame, spring perch, floor pan, and firewall.

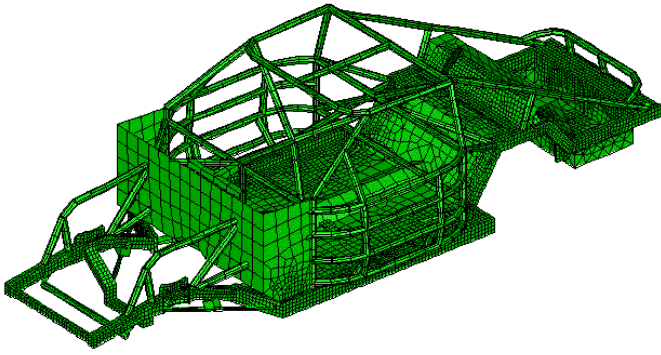


Figure 8. Full shell finite element mesh placed on surfaces of chassis frame.

To avoid these difficulties, yet enable the study of local deflections at the front suspension spring perches, an alternative modeling approach was used. In this alternative approach, beam elements are used to model all tubular members of the roll cage as well as box-beam frame rails away from the front suspension spring perches, while thin shell elements are used to model the front suspension spring perch/integrated frame rail assembly, see Figure 9. This approach reduced the number of DOF to model the chassis considerably. The local thin shell model of the perch is connected to the global beam model of the frame by joining dissimilar meshes of shell elements and beam elements using a “wheel” of rigid elements. The wheel of rigid elements is used to connect shell element nodes on the surface of the box beam adjacent to the spring perch with a node on the neutral axis of the beam representing the connecting frame rail. A study on the effectiveness of this modeling approach is given in [7], where it is shown that the beam/shell model asymptotically approaches the behavior of a full beam model for points sufficiently removed from the beam-mesh / shell-mesh transition area. Using this approach for joining dissimilar meshes ensures that local deflections observed at the front suspension spring perches are not modified by artificial local deflections at the beam/shell connection.

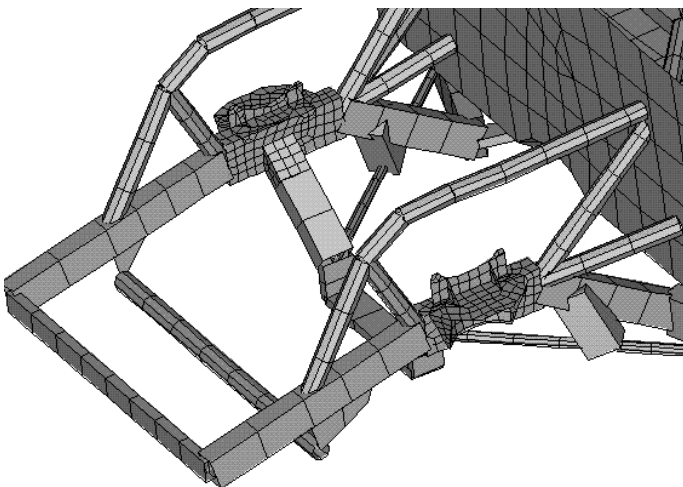


Figure 9. Global beam model of chassis frame rails coupled to local shell model of spring perch.

TORSIONAL STIFFNESS OF UNSUSPENDED CHASSIS

To analyze the torsional stiffness of an unsuspended chassis, the following boundary conditions are applied to the model. At the two rear spring mounts, the chassis is restrained in all three translations ($u_x = u_y = u_z = 0$), and lateral and vertical rotations ($\theta_y = \theta_z = 0$), while the longitudinal rotations at these points are free ($\theta_x = \text{free}$). These restraints are shown in Figure 10. At the front suspension spring mounts, equal and opposite vertical loads of 1000 lb_f are prescribed at node 1 and node 2. This loading is pictured in Figure 11. Results for roll and camber change by less than 1% using differential inputs in the opposite direction. These boundary conditions are representative of constraints applied by a twist fixture used by several race teams to measure torsional stiffness [2]. Recent studies given in [5] have shown that these restraints at the rear spring perches are “over-constrained” leading to torsional stiffness predictions which are elevated by 9% over the minimum constraint condition. However, for the purposes of this study, use of the boundary conditions described above is sufficient to predict relative changes in stiffness.

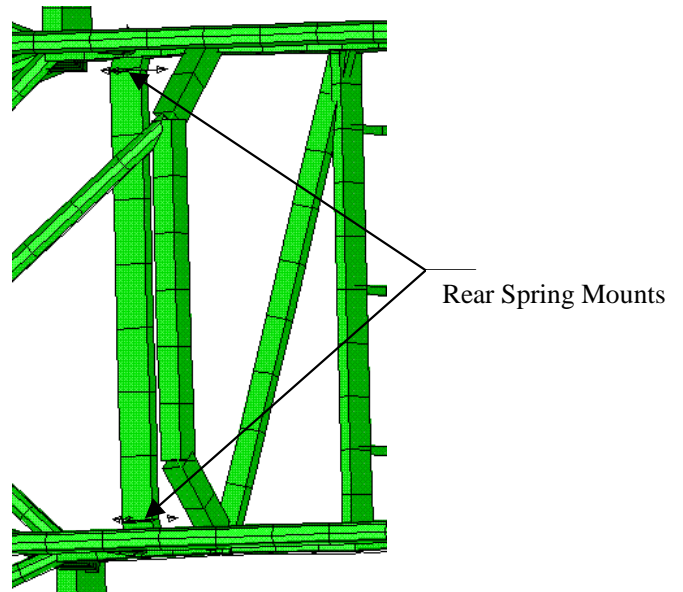


Figure 10. Rear spring mount restraints for torsional and roll stiffness tests.

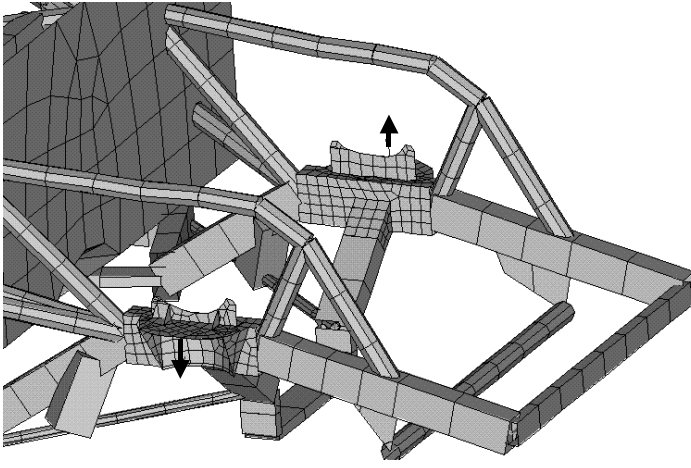


Figure 11. Equal and opposite vertical loads applied at front spring perches.

In the following, vector notation is used to define coordinates. Let \mathbf{x} represent the initial position vector, \mathbf{u} represent the displacement vector, with components (u_x, u_y, u_z) , and \mathbf{r} represent the deformed vector position such that $\mathbf{r} = \mathbf{x} + \mathbf{u}$. The position vector for point i is defined as $\mathbf{r}^{(i)}$, with coordinates $(r_x^{(i)}, r_y^{(i)}, r_z^{(i)})$. The distance between $\mathbf{r}^{(i)}$ and $\mathbf{r}^{(j)}$ measured in the Euclidean norm is then

$$\|\mathbf{r}^{(i)} - \mathbf{r}^{(j)}\| = \sqrt{(\Delta x_r)^2 + (\Delta y_r)^2 + (\Delta z_r)^2} \quad (\text{Eq. 1})$$

where

$$\Delta x_r = r_x^{(i)} - r_x^{(j)}$$

$$\Delta y_r = r_y^{(i)} - r_y^{(j)}$$

$$\Delta z_r = r_z^{(i)} - r_z^{(j)}$$

The displacement at point (i) is

$$\mathbf{u}^{(i)} = (u_x^{(i)}, u_y^{(i)}, u_z^{(i)})$$

The magnitude of \mathbf{u} is defined as

$$\|\mathbf{u}\| = \sqrt{u_x^2 + u_y^2 + u_z^2} \quad (\text{Eq. 2})$$

Similar notations are used for the initial position vector \mathbf{x} .

ANALYSIS OF UNSUSPENDED CHASSIS WITH FLEXIBLE FRONT SPRING PERCHES – In order to calculate torsional stiffness, the deflections of the front load/gauge points are related to the applied torque, given by $T = F \cdot d$, where F is the magnitude of the equal and opposite forces, and $d = 37.58''$ is the lateral distance between load points. Due to asymmetry within the chassis, the equal-and-opposite loading does not result in equal-and-opposite displacements. This behavior is illustrated in

Figure 12, where an initial configuration, defined by the positions of the left, $\mathbf{x}^{(1)}$, and right, $\mathbf{x}^{(2)}$, spring mounts, is deformed due to the equal and opposite forces F to the positions $\mathbf{r}^{(1)}$ and $\mathbf{r}^{(2)}$ respectively.

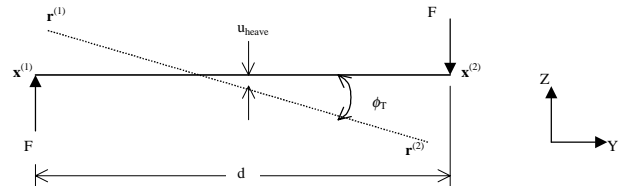


Figure 12. Deflection of spring mounts due to equal and opposite loads.

The chassis deflection can be characterized as the superposition of longitudinal roll ϕ_T and vertical heave, u_{heave} , defined by

$$u_{heave} = \frac{u_z^{(1)} + u_z^{(2)}}{2} \quad (\text{Eq. 3})$$

$$\phi_T = \arctan\left(\frac{\Delta z_r}{\Delta y_r}\right) \quad (\text{Eq. 4})$$

where

$$\Delta z_r = (r_z^{(2)} - r_z^{(1)})$$

$$\Delta y_r = (r_y^{(2)} - r_y^{(1)})$$

are the vertical and lateral distances between deflected spring mounts.

Torsional stiffness, K_T , is calculated from,

$$K_T = \frac{T}{\phi_T} \quad (\text{Eq. 5})$$

For the baseline Hopkins chassis with nominal perch thickness given in Table I, and with the constraints described earlier at the rear mounts, the torsional stiffness is calculated to be 9555 lb_f-ft/deg.

ANALYSIS OF UNSUSPENDED CHASSIS WITH RIGID FRONT SPRING PERCHES – To determine the maximum possible local stiffness, the front spring perches are modeled with infinitely rigid elements. The infinitely rigid perch is constructed by removing all shell elements from all surfaces on the spring perch. Next, all nodes except those that serve to connect the perch to the chassis and the suspension and those that are pertinent to measurement points are deleted. Finally, a rigid multi-point constraint element is created [1], rigidly linking all remaining nodes. Details for this rigid spring perch model are given in [7]. With rigid spring perches, the torsional stiffness is calculated to be $K_T = 11,576$ lb_f-ft/deg, an increase of 21% over the baseline chassis with flexible spring perches.

PARAMETRIC STUDIES OF UNSUSPENDED CHASSIS – In order to quantify the contributions of each member surface of the front suspension spring perch to the overall spring perch flexibility, parametric studies are performed by varying the thickness of the principal spring support plate, side gussets, and the frame rail spring pocket. Each plate thickness is varied over the range $t/t_{nom} = (0.25, 0.50, 0.75, 1, 2, 3, 4)$ where t_{nom} is the nominal thickness of the baseline chassis given in Table I. Two other configurations are also studied: an infinitely rigid spring perch assembly described earlier, and a spring perch assembly with only the surface of interest modeled as infinitely rigid (with other surface thicknesses being nominal). Flexibility is gauged by the torsional stiffness K_T , compared to a spring perch assembly with the surface of interest modeled as rigid.

EFFECTS OF SPRING SUPPORT PLATE FLEXIBILITY – The effects of principal spring support flexibility on chassis torsional stiffness is shown in Figure 13. The stiffness is normalized with the stiffness obtained with a rigid spring support plate.

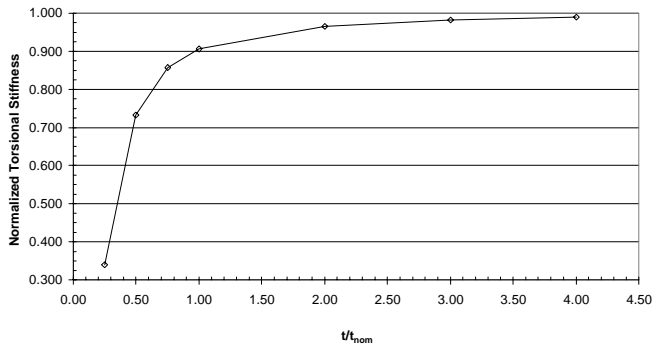


Figure 13. Normalized effects of Spring Plate Thickness on Torsional Stiffness of Unsuspended Chassis. Nominal thickness $t_{nom} = 0.39$ inches.

From these results, the flexibility of the spring support plate has a significant influence on the overall torsional stiffness of the chassis. As the thickness of the support plate increases, the stiffness approaches the asymptotic value of the rigid spring plate of $K_T = 10,537$ lb_f-ft/deg, an increase of approximately 10% over the nominal configuration. When the thickness is doubled to $t = 2 \times t_{nom}$, the global torsional stiffness increases by 6.5%. When the thickness is decreased from the nominal thickness, the global torsional stiffness decrease rapidly.

EFFECTS OF FRAME RAIL SPRING POCKET FLEXIBILITY – In this section, the effects of rigidity changes of the frame rail spring pockets are studied. These surfaces integrate with the frame rail box beam, the principal spring support plate, and the side gussets; see Figures 2 and 5. The impact of the rigidity of this surface on chassis torsional stiffness is plotted in Figure 14. The stiffness values are normalized with respect to the stiffness obtained with a rigid frame rail spring pocket.

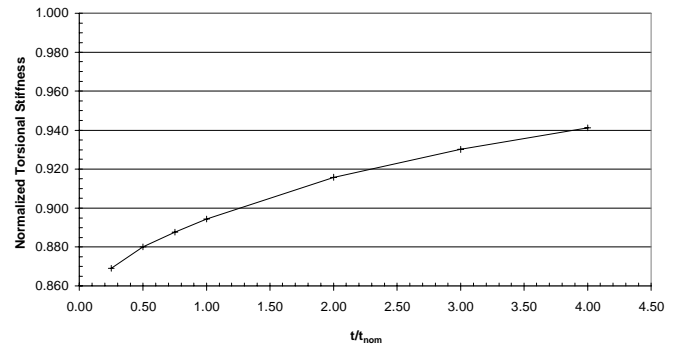


Figure 14. Normalized effects of frame rail spring pocket thickness on torsional stiffness. Nominal thickness $t_{nom} = 0.15$ inches.

The results indicate that the spring pocket has a large influence on chassis torsional stiffness; a rigid spring pocket would produce a torsional stiffness of 10,683 lb_f-ft/deg, representing an increase of 12% over nominal and only 8% less than the torsional stiffness for a fully rigid perch. However, in practice, to achieve a fully rigid spring pocket would require increasing the thickness to several times that of nominal, resulting in a substantial weight penalty. Doubling the pocket thickness to $t = 2 \times t_{nom}$ increases torsional stiffness by less than 2.5%, while decreasing to $t = t_{nom} / 2$ reduces torsional stiffness by only 2%.

EFFECTS OF FRAME RAIL BOX BEAM FLEXIBILITY – The last spring perch surface of concern when analyzing the effects of local flexibility on global behavior of the unsuspended chassis is the frame rail box beam. The effects of frame rail box beam thickness adjacent to the spring perch on the global torsional stiffness of the chassis is shown in Figure 15.

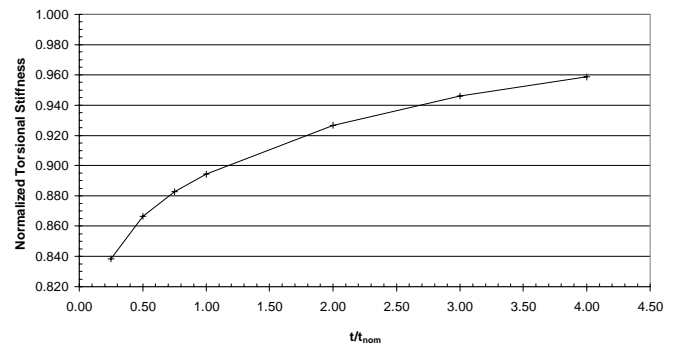


Figure 15. Normalized effects of frame rail box beam thickness on torsional stiffness. Nominal thickness $t_{nom} = 0.12$ inches.

These results show that significant improvements in torsional stiffness can be achieved by thickening or otherwise increasing the rigidity of the frame rail box beam adjacent to the spring perch. Doubling the wall thickness of the box beam increases torsional stiffness 3.6% (to 9900 lb_f-ft/deg). A rigid box beam raises torsional stiffness 13.5% over the existing spring perch assembly. A

rigid box beam enables a torsional stiffness of only 6.3% less than a fully rigid spring perch.

Other studies in [7] have shown that flexibility of the side gussets has only a small influence on the global chassis stiffness. A rigid side gusset increases torsional stiffness to 9963 lb-ft/deg, an increase of only 4% over the nominal thickness value. Decreasing the gusset thickness to 1/2 that of nominal lowers torsional stiffness by less than 1%.

CHASSIS WITH FRONT SUSPENSION MODEL

In this section, the effects of front spring perch flexibility on a baseline Hopkins chassis and front suspension are studied. These effects are quantified using the criteria of camber angle change, steer angle change, and effective roll stiffness. A finite element model of the front suspension was built and combined with the chassis model. The geometry of the suspension model is based on measured data taken from a Hopkins chassis supplied by one of the race teams [8]. The front suspension includes the upper and lower A-arms (control arms), suspension springs, spindles and sway bar assembly. The sway bar assembly includes the sway bar, sway bar support arms, and pivot links. The finite element model of the front suspension assembly is shown in Figure 16.

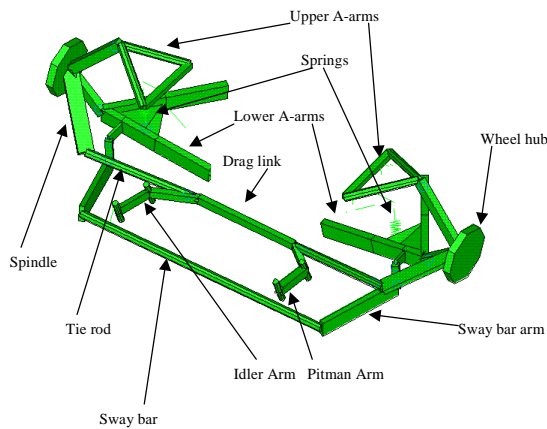


Figure 16. Front suspension components.

The locations of the wheel hubs, H , and wheel spindles, S , were measured for a typical Winston Cup racecar at ride height. The locations of these points measured in the global coordinate system are given in Table II. The static set-up parameters for each test of the Hopkins chassis with attached front suspension are summarized in Table III.

Table II. Key-nodes for front suspension analysis (global coordinate system).

Node	Description	x_x , in	x_y , in	x_z , in
13	Left Rear Spring Mount	102.175	-18.012	21.229
14	Right Rear Mount	102.254	16.983	21.813
15	Left Front Hub	-0.227	-30.033	13.300
16	Right Front Hub	-0.017	30.434	13.675
17	Left Front Inner Spindle	-0.227	-29.035	13.366
18	Right Front Inner Spindle	-0.017	29.436	13.610

Table III. Static set-up parameters for roll stiffness analysis

Parameter	Left	Right
Front Wheel Hub Center Height, in	13.2996	13.6749
Front Spring Rate, lb _f /in	1200	2000
Front Track Width, in	60.5	
Front Anti-Roll Bar Diameter, in	1.0	

The global coordinate system is oriented in the following manner: the x-axis is directed longitudinally from front to rear along the centerline of the car; the y-axis is oriented laterally, with positive directed to the right passing through the front wheel centers; and the z-axis is vertical (positive up). This coordinate system is chosen for convenience, as it is the same as the coordinates used by Day [8] to measure the suspension geometry. This coordinate system is different from the standard SAE reference frame centered at the “sprung mass” center of gravity (cg).

In order to model the hinge joint connecting the upper A-arms to the support bracket of the spring perch, coupled degrees-of-freedom were used, see Figure 17. A local coordinate system is used to align the hinge connection. A linear spring element is used to model the coil spring mounted between the upper spring perch and lower A-arm.

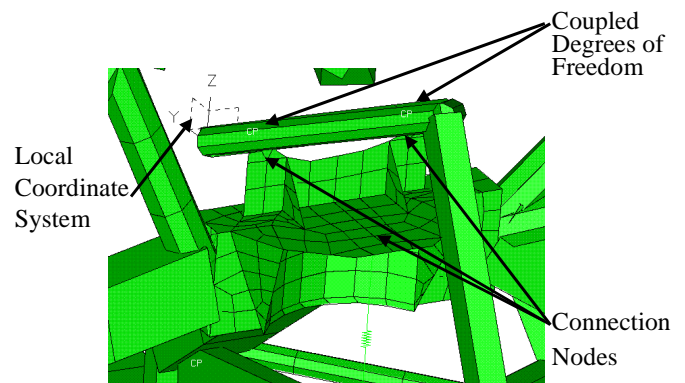


Figure 17. Suspension attachments to front spring perch.

The complete chassis/suspension finite element model is shown in Figure 18. Details for the geometry and other connections of the suspension to the chassis frame are given in [9].

The following assumptions were made for the chassis/suspension model:

- The material is assumed linear elastic and calculations are performed using linear static finite element analysis with small deformations resulting in constant stiffness predictions.
- The coil springs are modeled using linear spring elements with constant spring rates.
- The wheel travel due to vertical inputs is small resulting in small deflections from the design position.

To validate the chassis/suspension FEM model, results from a static “jack test” were compared to measured data in [8]. The “jack test” consists of applying a vertical load using hydraulic jack on the left frame rail of the chassis, simulating vehicle roll to the right as occurs in a left-hand turn. The changes in normal wheel load due to the jack force for each tire predicted by the FEM and measured test data agreed within 1.7 % [7].

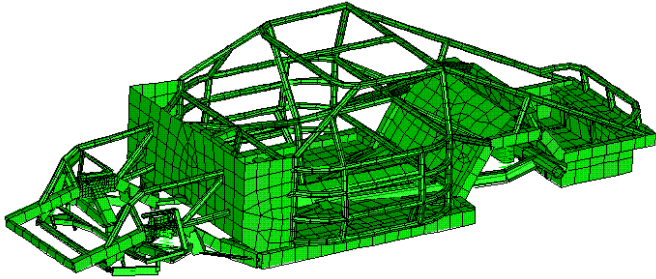


Figure 18. Complete chassis/suspension finite element model.

Effective front roll stiffness, and camber and steer response of the suspension with flexible spring perches is determined based on differential vertical load inputs at the front wheel hub centers. The model allows for small deflections only and predicts changes in roll stiffness, camber and steer response due to changes in chassis stiffness. Specifically, the vertical wheel travel allowed due to the vertical inputs is small resulting in camber and steer response due to changes in stiffness. Torque is applied from differential load inputs at the front wheel hubs (nodes 15 and 16); see Figure 19. The two rear spring mounts on the chassis are restrained in the same manner as for the torsional stiffness analysis; ($u_x = u_y = u_z = 0$), ($\theta_y = \theta_z = 0$), with ($\theta_x = \text{free}$). The global coordinates of the front and rear boundary condition nodes are given in Table II. Symmetry is not present between the left- and right-hand side coordinates due to the initial roll (wedge) of the chassis at race height.

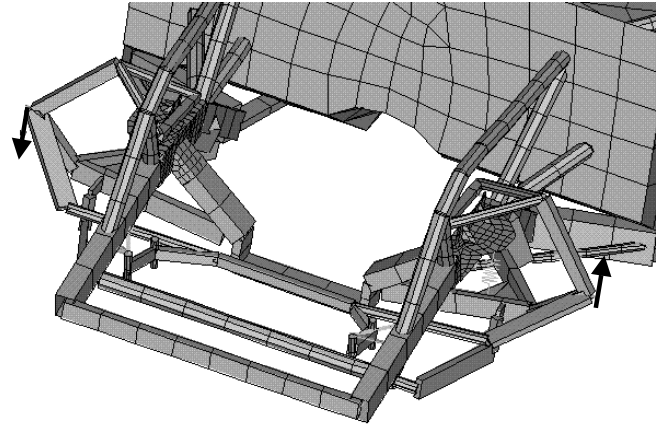


Figure 19. Equal and opposite forces applied at wheel hubs.

FRONT ROLL STIFFNESS – In order to calculate roll stiffness, the deflections of the wheel hubs are related to the torque applied at these locations. As the applied forces are of equal magnitude and opposite direction, the net force applied to the system is zero. The applied torque is calculated from $T = F \times d_R$, where d_R is the lateral distance between wheel hub centers,

$$d_R = x_y^{(16)} - x_y^{(15)} = 60.47\text{in} \quad (\text{Eq. 6})$$

The initial roll angle due to wedge is calculated from,

$$\phi_i = \arctan\left(\frac{\Delta z_x}{\Delta y_x}\right)$$

where

$$\begin{aligned} \Delta z_x &= \mathbf{x}_z^{(16)} - \mathbf{x}_z^{(15)} \\ \Delta y_x &= \mathbf{x}_y^{(16)} - \mathbf{x}_y^{(15)} \end{aligned}$$

The wheel hubs deflect under the differential load input to positions $\mathbf{r}^{(15)}$ and $\mathbf{r}^{(16)}$. Consistent with the linear finite element analysis, these deflections are small. The change in roll angle from the initial roll angle is calculated from,

$$\Delta\phi_R = \arctan\left(\frac{\Delta z_r}{\Delta y_r}\right) - \phi_i \quad (\text{Eq. 7})$$

where

$$\begin{aligned} \Delta z_r &= \mathbf{r}_z^{(16)} - \mathbf{r}_z^{(15)} \\ \Delta y_r &= \mathbf{r}_y^{(16)} - \mathbf{r}_y^{(15)} \end{aligned}$$

Based on the deflected coordinates and the applied torque, the effective roll stiffness of the front suspension in combination with the flexible chassis is,

$$K_R = \frac{F \cdot d_R}{\Delta\phi_R} = 1926.5 \frac{\text{lb}_f \cdot \text{ft}}{\text{deg}} \quad (\text{Eq. 8})$$

The above formulas may be compared to Soni [9]. Expanding equation (7), we have:

$$\Delta\phi = \arctan\left(\frac{\Delta z_r}{\Delta y_r}\right) - \arctan\left(\frac{\Delta z_x}{\Delta y_x}\right)$$

Employing the small angle approximation ($\tan \alpha \approx \alpha$) gives

$$\Delta\phi \approx \left(\frac{\Delta z_r}{\Delta y_r}\right) - \left(\frac{\Delta z_x}{\Delta y_x}\right)$$

For small deflections, $u_y^{(15)} \approx u_y^{(16)} \approx 0$, it follows that $\Delta y_r \approx \Delta y_x$. Combining fractions over a common denominator of Δy_x , and recognizing that $\Delta y_x = d_R$ yields:

$$\begin{aligned} \Delta\phi &\approx \frac{\Delta z_r - \Delta z_x}{d_R} \\ &\approx \frac{\Delta u_z}{d_R} \end{aligned}$$

Placing this value of $\Delta\phi$ into equation (4.3) yields:

$$\begin{aligned} K_R &= \frac{F \cdot d_R}{\frac{\Delta u_z}{d_R}} \\ &= \frac{F \cdot d_R^2}{\Delta u_z} \end{aligned}$$

which is similar to Soni [9]. Calculating roll stiffness by this formula yields $K_R = 1928 \text{ lb}_f\text{-ft/deg}$. This difference shows that for the small deformations assumed in the analysis, the lateral deflections (u_y) of the wheel hubs are negligible in the computation of roll stiffness.

CAMBER – An important parameter in the handling of a race car is camber. Tire camber angle is a function of the vertical displacement of the chassis and the steer angle of each tire [6]. The sign convention for camber is such that positive camber results in the top of the tire tilting outward from the vehicle centerline and negative camber results in the tire tilting inward. Defining the wheel local vertical as the line from the wheel hub center to the “top” point on the outside edge of the wheel/tire, γ , represents the angle between the global vertical line and the wheel local vertical; this is depicted in Figure 20.

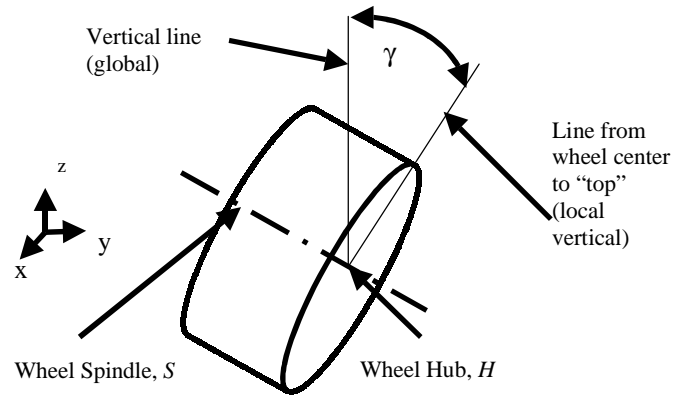


Figure 20. Definition of camber.

Camber angle is defined as:

$$\gamma = \arcsin\left(\frac{S_z - H_z}{\sqrt{(S_x - H_x)^2 + (S_y - H_y)^2 + (S_z - H_z)^2}}\right)$$

The initial camber for the left tire is

$$\gamma_i^L = \arcsin\left(\frac{\Delta z_x}{\|\mathbf{x}^{(17)} - \mathbf{x}^{(15)}\|}\right) = +3.819^\circ$$

where

$$\begin{aligned} \Delta z_x &= x_z^{(17)} - x_z^{(15)} \\ \gamma_i^R &= \arcsin\left(\frac{\Delta z_x}{\|\mathbf{x}^{(18)} - \mathbf{x}^{(16)}\|}\right) = -3.721^\circ \end{aligned} \quad (\text{Eq. 1})$$

where

$$\Delta z_x = x_z^{(18)} - x_z^{(16)}$$

After the small deformation due to the differential load inputs, the wheel spindles deflect to positions, $\mathbf{r}^{(17)}$ and $\mathbf{r}^{(18)}$. The change in camber due to the applied torque is the difference between the deflected and initial configurations.

For the left wheel,

$$\Delta\gamma = \arcsin\left(\frac{\Delta z_r}{\|\mathbf{r}^{(17)} - \mathbf{r}^{(15)}\|}\right) - \gamma_i^{(L)}$$

where

$$\Delta z_r = r_z^{(17)} - r_z^{(15)}$$

For the right wheel,

$$\Delta\gamma = \arcsin\left(\frac{\Delta z_r}{\|\mathbf{r}^{(18)} - \mathbf{r}^{(16)}\|}\right) - \gamma_i^{(R)}$$

where

$$\Delta z_r = r_z^{(18)} - r_z^{(16)}$$

Camber response to differential load input is given by $1/K_C$, where

$$K_C = \frac{F \cdot d_R}{|\Delta\gamma|}$$

is a “camber stiffness” parameter. For the baseline chassis with attached front suspension, the left front camber stiffness is $K_C = 2597 \text{ lb}_f\text{-ft/deg}$, and the right is $K_C = 2796 \text{ lb}_f\text{-ft/deg}$.

STEER ANGLE – Another important parameter that affects handling is the steer angle of the front wheels. Steer angle, denoted in this paper by β , is defined as the angle between the longitudinal axis of the wheel (front-to-rear) and the longitudinal axis of the chassis. The notation β used in this paper for steer angle is different than the commonly used symbol δ . Alternately, steer angle may be viewed as the angle between the wheel spin axis and the global lateral axis in the global horizontal plane. Steer angle is depicted in Figure 21.

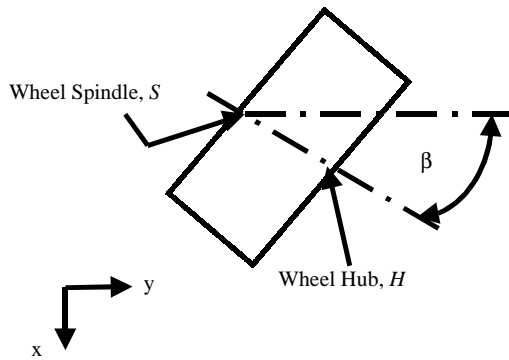


Figure 21. Definition of steer angle.

The steer angle is defined as:

$$\beta = \arctan\left(\frac{S_z - H_z}{S_y - H_y}\right)$$

A positive angle represents steer to the right [6]. For the suspension geometry used in this study, there is no initial steer angle. Steer response to differential load input is given by $1/K_S$, where

$$K_S = \frac{T_R}{\beta}$$

is a “steer stiffness” parameter. The baseline chassis with front suspension yields a left steer angle stiffness of $K_S = 28,394 \text{ lb}_f\text{-ft/deg}$, while the right wheel exhibits a steer angle stiffness of $K_S = 22,101 \text{ lb}_f\text{-ft/deg}$.

Results for the flexible spring perch are compared to results for a rigid spring perch. Based on the calculated deflections from the applied torque, the effective front roll stiffness of the chassis/ suspension assembly with rigid spring perch is $K_R = 1991 \text{ lb}_f\text{-ft/deg}$. This stiffness represents an increase of 3.4% over the flexible spring perch model.

PARAMETRIC STUDIES OF CHASSIS/ FRONT SUSPENSION – In order to quantify the contributions of each member surface of the front suspension spring perch to the overall chassis / front suspension behavior, parametric studies are performed by varying the thickness of the spring support plate, side gussets, frame rail spring pocket, upper A-arm attachment plate support brackets, upper A-arm attachment plate ears, and upper A-arm attachment plate bases. Each plate thickness is varied over the range $t/t_{nom} = (0.25, 0.50, 0.75, 1, 2, 3, 4)$ where t_{nom} is the nominal thickness of the baseline chassis given in Table I. Two other configurations are also studied: an infinitely rigid spring perch assembly, and a spring perch assembly with only the surface of interest modeled as infinitely rigid (with other surface thicknesses being nominal).

EFFECTS OF SPRING SUPPORT PLATE FLEXIBILITY – The first surface to be analyzed is the principal spring support plate. The effects of spring plate thickness on roll stiffness is shown in Figure 22. Camber angle change, normalized with the camber angle response for the rigid spring plate case, $|\Delta\gamma| / |\Delta\gamma|_{rigid}$, is plotted as a function of plate thickness in Figure 23.

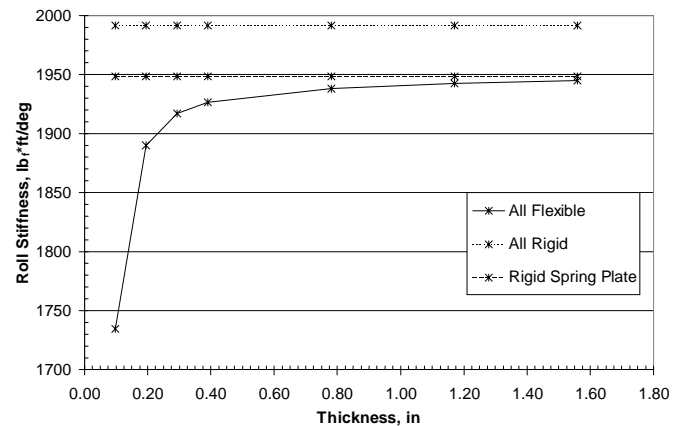


Figure 22. Effects of principal spring support plate thickness on roll stiffness ($t_{nom} = 0.39 \text{ in}$).

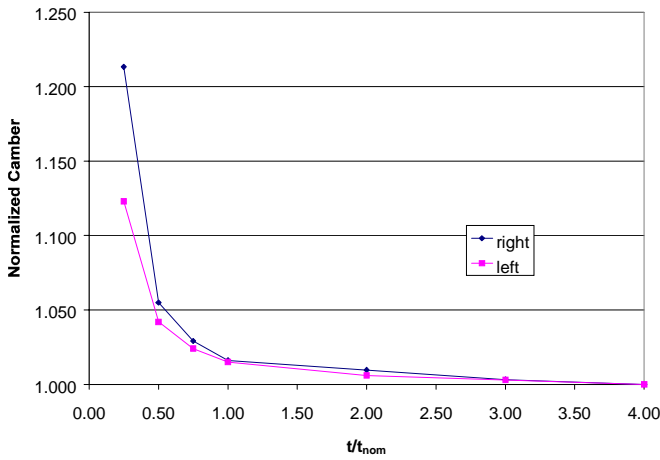


Figure 23. Effects of principal spring support plate thickness on camber angle change ($t_{nom} = 0.39$ in).

The results show that roll stiffness decreases by 10% compared to nominal when the thickness is reduced to $t = t_{nom} / 4$, while thickening the support plate to $t = 4 \times t_{nom}$, increases roll stiffness by less than 1%. From this result, it appears that the nominal thickness value is sufficient to maintain the roll stiffness designed for the suspension system. Increasing thickness does not change roll stiffness significantly, yet decreasing thickness below nominal produces a substantial decrease in effective roll stiffness.

Similar behavior is exhibited for the wheel camber response. Decreasing thickness to $0.25t_{nom}$ decreases the normalized camber angle significantly, to 12% of the for the left and 21% for the right compared to camber change for the rigid plate case. The normalized camber angle change is less than 1.5% for both left and right wheels at nominal plate thickness. Results given in [9] show that increasing or decreasing principal spring support plate thickness from $0.25t_{nom} \leq t_{nom} \leq 4t_{nom}$ has negligible effect on steer angle.

EFFECTS OF FRAME RAIL SPRING POCKET FLEXIBILITY – The next surface studied is the frame rail spring pocket. Roll stiffness versus spring pocket thickness is plotted in Figure 24. The relationship between normalized camber angle change $|\Delta\gamma| / |\Delta\gamma|_{rigid}$, and spring pocket thickness is shown in Figure 25. Steer angle, normalized with the steer angle response for the rigid spring pocket case, β / β_{rigid} , is plotted as a function of plate thickness in Figure 26.

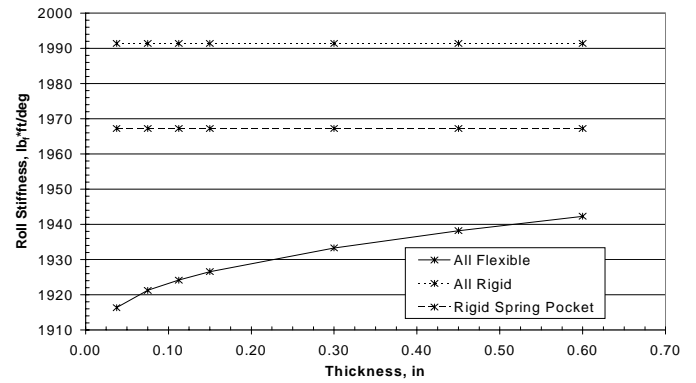


Figure 24. Effects of frame rail spring pocket flexibility on roll stiffness.

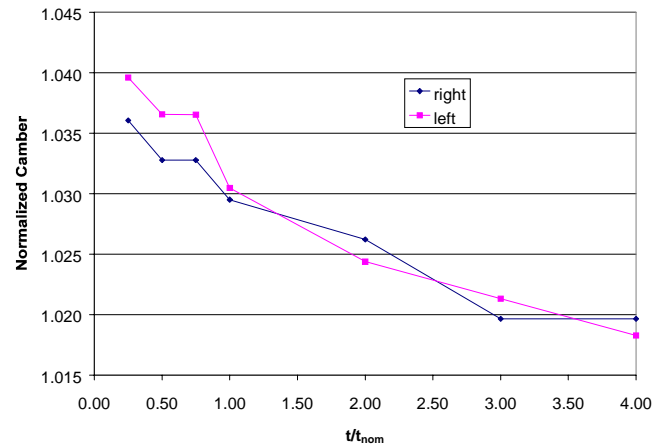


Figure 25. Effects of frame rail spring pocket flexibility on camber angle change.

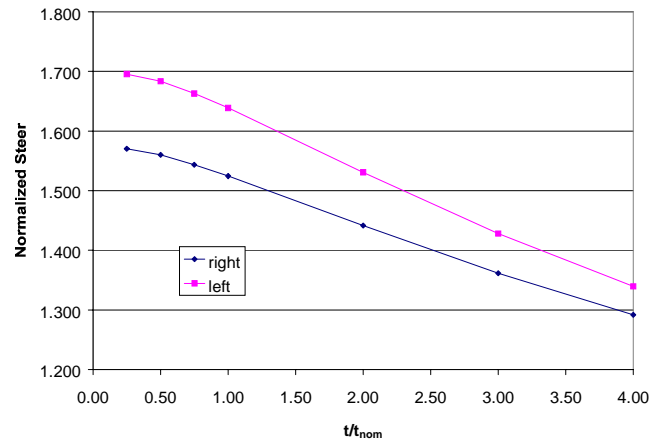


Figure 26. Effects of frame rail spring pocket flexibility on steer angle.

Roll stiffness increases modestly with increasing thickness of the frame rail spring pockets. The study suggests that a rigid spring pocket would raise roll stiffness to 1967 lb_f-ft/deg (an increase of 2.1% over the nominal configuration). However, increasing the thickness of this surface to four times nominal yields a roll stiffness of only 1942.3 lb_f-ft/deg (an increase of 0.8% over the standard configuration). Making only the spring pocket rigid gives a roll stiffness value that is 98.8% of that possible with an entirely rigid spring perch structure.

Camber angle change is very consistent when compared with increasing spring pocket thickness. Decreasing spring pocket thickness to 25% of nominal lowers camber angle only 1.5% compared to nominal and 1.0% compared to nominal for the left and right-sides respectively.

Steer angle changes steadily decrease with increase in spring pocket thickness. For nominal thickness, the steer angle change is 53% for the left and 43% for the right from the rigid spring pocket response. Over the thickness range studied, steer angle changes are significantly higher than those resulting from a completely rigid spring perch assembly.

EFFECTS OF SIDE GUSSET FLEXIBILITY – Results given in [7] indicate that the flexibility of the side gussets has little effect on the effective roll stiffness of the front suspension. Changes in side gusset thickness change roll stiffness by less than 0.6% over the range studied. Similar behavior is exhibited for camber and steer angles – side gusset flexibility has little effect.

EFFECTS OF UPPER A-ARM ATTACHMENT PLATE SUPPORT BRACKET FLEXIBILITY – From the results given in [7], the upper A-arm attachment plate support brackets also play little role in determining front roll stiffness. The roll stiffness would only increase 0.22% (to 1931 lb_f-ft/deg) if these surfaces were rigid. Roll stiffness only decreases 0.03% (to 1925.9 lb_f-ft/deg) when these members lose 75% of their thickness. Camber angle change is also very consistent; the nominal thickness produces camber angle values which are within 0.5% of the rigid support bracket value on the left and equivalent to the rigid support bracket value on the right. As these brackets are supporting the upper A-arm attachment plate, they do play a major role in maintaining the local stiffness of the upper A-arm attachment plates.

EFFECTS OF UPPER A-ARM ATTACHMENT PLATE BASE FLEXIBILITY – From the results given in [7], the upper A-arm attachment plate base thickness also plays a minor role in determining roll stiffness. The base is differentiated from the top of the upper A-arm attachment plate since it is not reinforced by shims. Camber and steer angles increase slightly on each side if this plate is thinned, but the benefits resulting from increasing this plate thickness are minimal.

EFFECTS OF FRAME RAIL BOX BEAM FLEXIBILITY – The last surface to be investigated in this study are the frame rail box beams. The effects of the box beam wall thickness on roll stiffness are plotted in Figure 27. The effects of the box beam rigidity on camber and steer are plotted in Figures 28 and 29.

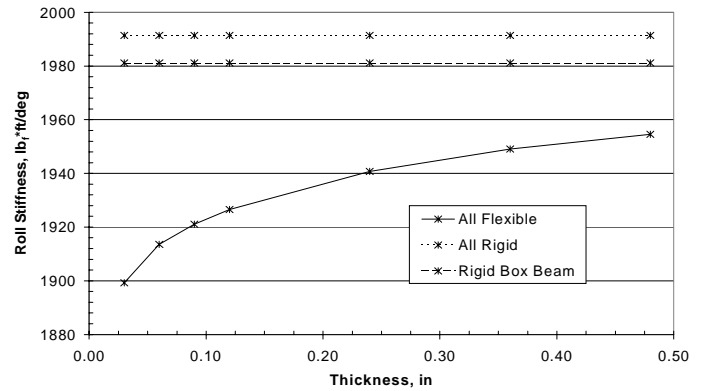


Figure 27. Effects of frame rail box beam flexibility on roll stiffness.

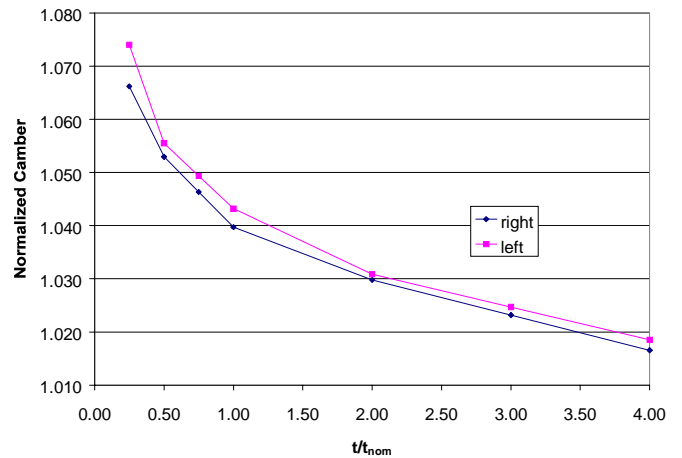


Figure 28. Effects of frame rail box beam flexibility on camber angle change.

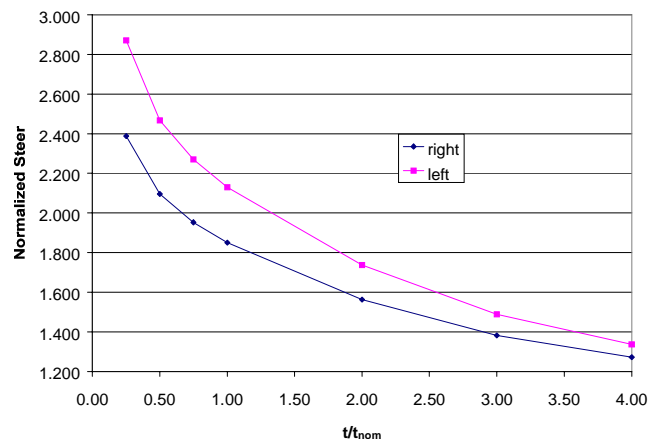


Figure 29. Effects of frame rail box beam flexibility on steer angle.

A rigid box beam increases roll stiffness 2.8% (to 1981 lb_f-ft/deg), but increasing the box beam wall thickness 300% increases roll stiffness only 1.5% (to 1955 lb_f-ft/deg). Decreasing box beam wall thickness by 75% decreases roll stiffness by only 1.5% (to 1899 lb_f-ft/deg).

SUMMARY OF THE EFFECTS OF DECREASED SPRING PERCH THICKNESS – From the results of this study, we found that the thickness of different surfaces of the spring perch had varying influence on suspension behavior. The effects of thinning each of the seven parametric surfaces of the spring perch on camber angle, roll angle, and steer angle are summarized in Table IV by computing the relative difference between each angle for a nominally-configured spring perch versus a spring perch with one surface of thickness $0.25t_{nom}$ and all other surfaces with thickness t_{nom} . Camber and steer are given as the average of the left and right wheels. These results are presented graphically in Figure 30.

Table IV. Relative difference between angle changes using (t_{nom}) and ($0.25 t_{nom}$).

Surfaces	Camber	Roll	Steer
Spring Plates	15.02%	11.08%	-2.25%
Box Beam	2.74%	1.44%	32.10%
Attachment Plate Base	2.86%	0.55%	-7.59%
Spring Pockets	0.76%	0.53%	3.27%
Side Gussets	0.31%	0.10%	-1.66%
Attachment Plate Ear	0.76%	0.09%	-0.98%
Support Brackets	0.14%	0.03%	-0.18%

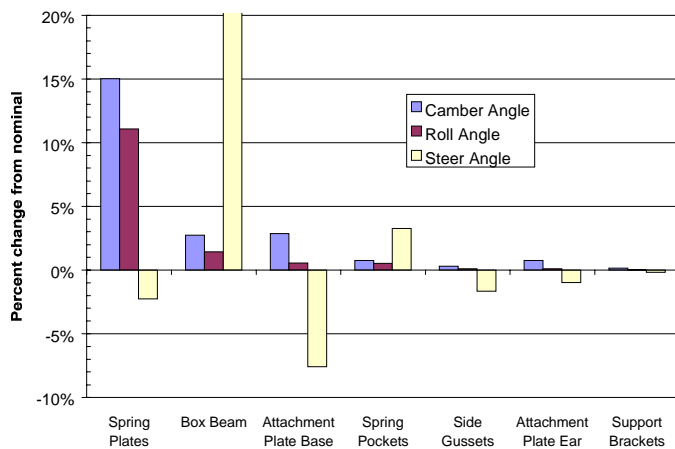


Figure 30. Angle change comparison for each surface with thickness $0.25t_{nom}$ versus nominal thickness.

From Table IV it can be seen that the thickness of the principal spring support plates should not be reduced from nominal, as roll and camber response are changed severely. Thinning the box beam walls adversely affects all the parameters. Thinning the frame rail spring pocket will also change steer angle response.

SUMMARY OF THE EFFECTS OF INCREASED SPRING PERCH THICKNESS – In order to determine which surfaces would benefit from thickening, results for the relative angle change due to increasing surface thickness to four times nominal is summarized. The relative difference between angle changes using nominal and four times nominal thickness for each surface is given in Table V. Figure 31 shows a bar graph representation of this data.

Table V. Relative difference between angle changes using (t_{nom}) and ($4.00 t_{nom}$).

Surfaces	Camber	Roll	Steer
Box Beam	-2.29%	-1.44%	-34.73%
Spring Plates	-1.54%	-0.95%	-6.26%
Spring Pockets	-1.07%	-0.81%	-16.97%
Side Gussets	-0.45%	-0.28%	-1.24%
Attachment Plate Base	-0.31%	-0.20%	1.03%
Support Brackets	0.00%	-0.12%	0.49%
Attachment Plate Ear	0.14%	-0.02%	0.01%

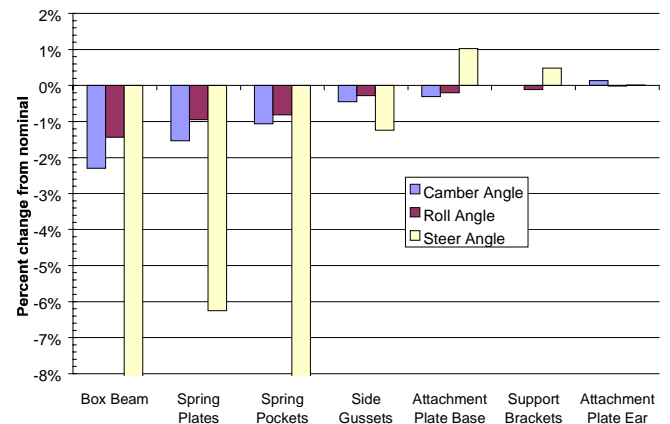


Figure 31. Angle change comparison for each surface with thickness $4.00t_{nom}$ versus nominal thickness.

In the above table and chart, it can be seen that the box beam walls, spring plates, and spring pockets benefit most from thickening. The box beam wall thickness and spring pocket thickness greatly influence steer angle response, and affects camber roll to a lesser degree. Spring plate thickness decreases changes in steer angle significantly; it also decreases roll and camber angles slightly.

SUMMARY OF THE EFFECTS OF MAKING SPRING PERCH SURFACES RIGID – Table VI shows the influence one rigid surface has compared to the nominal spring perch configuration. These results are graphed in Figure 33.

Table VI. Relative difference between angle changes using (rigid) and (nominal) thickness.

Surfaces	Camber	Roll	Steer
All Rigid	-5.23%	-3.26%	-49.26%
Box Beam	-3.97%	-2.76%	-50.19%
Spring Pockets	-2.91%	-2.07%	-37.06%
Spring Plates	-1.54%	-1.14%	-9.36%
Side Gussets	-0.76%	-0.50%	-3.79%
Attachment Plate Base	-0.61%	-0.28%	1.29%
Support Brackets	-0.14%	-0.22%	0.84%
Attachment Plate Ear	0.00%	-0.05%	0.92%

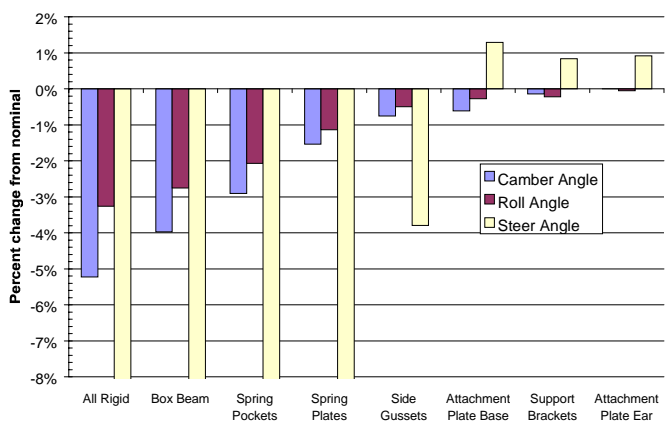


Figure 33. Angle changes comparison for each surface with infinite rigidity versus nominal rigidity.

The table and graph above show that making only the frame rail box beam rigid nearly replicates the results of an entire rigid perch in all aspects. Steer angle changes are greatly reduced by making the spring pocket rigid. Significant reductions in camber and roll angle changes are also achieved by making the spring pocket rigid. All of the above tables show that the upper A-arm attachment plate support brackets and attachment ear/ shim assemblies contribute the least to the roll, camber, and steer measures.

CONCLUSIONS AND RECOMMENDATIONS

Linear finite element analysis has been employed to analyze the effects of spring perch flexibility on the behaviour of a Winston Cup racecar chassis. Details such as side gussets, supporting brackets, and local curvature of the frame rail spring pocket are included in a shell model of

the spring perch. The local shell model of the spring perch is integrated with the global finite element stiffness model of the chassis and suspension consisting of an assembly of beam and shell elements. Care has been taken to model the connection between the local shell model and the global chassis model using rigid elements, i.e. multi-point constraints. The use of a local/global model of the perch/chassis reduces significantly the computational resources required to accurately model the local flexibility of the spring perch together with the overall global stiffness of the chassis.

Local stiffness within the front suspension spring perches was controlled by individually varying the thickness of each of the seven surfaces that comprise the spring perches: separate test cases were examined where one surface was rigid while all others had nominal thickness and rigidity. A completely rigid perch assembly was also studied.

Effective roll stiffness, camber and steer response, of the suspension with flexible chassis is determined based on differential vertical load inputs at the front wheel hub centers. The model allows for small deflections only and based on linear finite element analysis predicts changes in roll, camber, and steer response due to changes in chassis stiffness. Specifically, the vertical wheel travel allowed due to the vertical inputs is small resulting in camber and steer response due to changes in stiffness.

Major results from the study include the following:

- If making only one surface rigid, the frame rail box beam walls achieve the greatest benefits for reducing changes in roll, camber, and steer response. Increasing thickness approaches the rigid case rather slowly. Decreasing box beam wall thickness causes steer angle deflections to increase substantially.
- For the “auxiliary” spring perch surfaces (i.e., all surfaces studied except the frame rail box beam), the frame rail spring pockets are most important to increase rigidity. Steer angle changes decrease significantly when the spring pocket is rigid.
- The thickness of the principal spring support plate should not be lessened, as roll and camber changes increase rapidly. The spring plates approach rigid behavior with a thickness of four times nominal.
- The upper A-arm attachment plate base and side gussets have minor influences on each parameter. The upper A-arm attachment plate ear/ shims and support brackets have negligible influences on each parameter.
- As it has been shown the most influential surfaces on each parameter are the frame rail box beam and frame rail spring pocket, structural reinforcement efforts should focus on internal bracing and gusseting amongst these surfaces. It was also shown that merely thickening these members does not provide great stiffness benefits for the global structure.

In summary, the results from this study indicate that the local front spring perch stiffness of a typical Winston Cup chassis, such as the baseline Hopkins chassis would be reduced significantly with reduction in thickness of the frame rail box beam walls and principal spring support plates. This decrease in local stiffness would impact torsional stiffness and roll stiffness, as well as camber and steer angle changes. This study has also shown the tremendous importance of maintaining the stiffness of the frame rail box beam. When considering only the auxiliary spring perch surfaces (i.e., those that are welded to the original frame rail box beam), the stiffness of the frame rail spring pocket is very important. While the existing design is very good, structural benefits may be attained by increasing the rigidity of the frame rail box beam walls and spring pockets. These box beam walls and spring pockets should be fortified through internal bracing and gussets.

Further useful work would be to determine torsional stiffness of the chassis, including the detailed model of spring perches and the suspension, by removing the sway bar, modeling infinite springs and loading differentially thru the wheel hubs instead of at the chassis spring mounts. Other useful measures would be to determine camber and steer response to a lateral force at the ground contact point. Using the finite element model developed in this work as a basis, we are currently performing analysis of these commonly used measures and will report results in a future manuscript.

ACKNOWLEDGEMENT

We would like to thank Pipasu Soni for providing the suspension model used in this work. We would also like to thank the reviewers of this manuscript for useful comments and suggestions.

REFERENCES

1. Integrated Design Engineering Analysis Software Master Series 5, Computer Software. Structural Dynamics Research Corporation, 1997.
2. Keiner, Henning. "Static Structural Analysis of a Winston Cup Chassis under a Torsional Load". Report # TR-95-100-ME-MSP. Department of Mechanical Engineering, Clemson University, 1995.
3. John Crawford, "Finite Element Analysis of a NASCAR Winston Cup Stock Car", SAE Paper No. 942527, SAE Motorsports Engineering Conference, Detroit, MI, December 1994.
4. Raju, Srikanth. "Design and Analysis of a Winston Cup Stock Car Chassis for Torsional Stiffness using the Finite Element Method", Master of Science Thesis, Department of Mechanical Engineering, Clemson University, August 1998.
5. Lampert, Jon K. "Design and Analysis of a Twist Fixture to measure the Torsional Stiffness of a Winston Cup Chassis", Master of Science Thesis, Department of Mechanical Engineering, Clemson University, August 1998.
6. Milliken, Douglas L. and William F. Milliken. Race Car Vehicle Dynamics. Pennsylvania: SAE Publications Group, 1995.
7. Day, Kent A. Doctor of Philosophy Dissertation. Department of Mechanical Engineering, Clemson University, in preparation.
8. Herrick, Gregory, P. "The Effects of Spring Perch Flexibility on Front Suspension Geometry and Roll Stiffness of a Winston Cup Stock Car Using the Finite Element Method", Master of Science Thesis. Department of Mechanical Engineering, Clemson University, August 1998.
9. Soni, Pipasu H. "Effects of Chassis Flexibility on Roll Stiffness of a Winston Cup Stock Car Using the Finite Element Method". Master of Science Thesis. Department of Mechanical Engineering, Clemson University, May 1998.